

Annual Review of Biophysics

The Physics of the Metaphase Spindle

David Oriola,^{1,2,3} Daniel J. Needleman,⁴
and Jan Brugués^{1,2,3}

¹Max Planck Institute of Molecular Cell Biology and Genetics, 01307, Dresden, Germany; email: brugues@mpi-cbg.de

²Max Planck Institute for the Physics of Complex Systems, 01187, Dresden, Germany

³Center for Systems Biology Dresden, 01307, Dresden, Germany

⁴School of Engineering and Applied Sciences, Department of Molecular and Cellular Biology, and FAS Center for Systems Biology, Harvard University, Cambridge, Massachusetts 021382, USA



**ANNUAL
REVIEWS Further**

Click here to view this article's online features:

- Download figures as PPT slides
- Navigate linked references
- Download citations
- Explore related articles
- Search keywords

Annu. Rev. Biophys. 2018. 47:655–73

The *Annual Review of Biophysics* is online at biophys.annualreviews.org

<https://doi.org/10.1146/annurev-biophys-060414-034107>

Copyright © 2018 by Annual Reviews.
All rights reserved

Keywords

mitotic spindle, molecular motors, microtubules, kinesin, dynein, active gel theory

Abstract

The assembly of the mitotic spindle and the subsequent segregation of sister chromatids are based on the self-organized action of microtubule filaments, motor proteins, and other microtubule-associated proteins, which constitute the fundamental force-generating elements in the system. Many of the components in the spindle have been identified, but until recently it remained unclear how their collective behaviors resulted in such a robust bipolar structure. Here, we review the current understanding of the physics of the metaphase spindle that is only now starting to emerge.

Contents

1. INTRODUCTION	656
2. MICROTUBULE DYNAMICS.....	658
3. SPINDLE ARCHITECTURE.....	660
4. MICROTUBULE NUCLEATION.....	662
5. SPINDLE MECHANICS.....	663
5.1. Spindle Rheology.....	664
5.2. The Spindle as an Active Liquid Crystal.....	666
6. OUTLOOK.....	667

1. INTRODUCTION

Cell division results from the orchestrated organization of intracellular structures and molecules inside the cell. At the end of the nineteenth century, Flemming (28) described the shape and behavior of the mitotic spindle, a complex structure that segregates chromosomes during cell division. In the 1950s, seminal studies by Inoué (50) using polarization microscopy showed that the spindle was composed of filaments running along the spindle axis. Such fibers (later identified as microtubules) were proposed to generate mechanical force through polymerization/depolymerization dynamics (51), the molecular basis of which began to be revealed with the finding that microtubules are composed of the protein tubulin (8). The discovery of spindle microtubule cross-bridges in electron microscopy (47) motivated the proposal of a sliding filament mechanism for mitosis (72), inspired by the sliding filament model in skeletal muscle contraction (49). The relative importance of microtubule polymerization/depolymerization dynamics and motor-induced microtubule sliding was fiercely debated, eventually settling on the modern view that both processes are crucial for spindle form and function. Seminal studies of Bruce Nicklas on the necessary force to stall chromosomes during anaphase highlighted the force-generating capacity of the spindle machinery and the importance of mechanics in understanding spindle assembly (4, 89, 90). In the early 1990s, the role of motor proteins in mitosis was clearly revealed by genetic analysis (26, 73, 100). A tetrameric kinesin was identified to drive microtubule cross-linking (60) and cytoplasmic dynein was shown to drive minus end clustering in taxol-induced aster formation (122). Kinesins were later found to also be involved in polar ejection forces acting on chromosomes (12, 99), and many members of the kinesin superfamily are known to play major roles in spindle assembly and maintenance (17, 96). The list of proteins involved in spindle assembly is widely believed to be close to complete (17, 62, 102, 129), but how these proteins self-organize to generate forces and shape the spindle is still poorly understood (24, 54, 59).

The spindle apparatus is a highly dynamic structure: All of its microtubules turn over every ~ 30 s. This feature makes the spindle challenging to study, from both physical and biological perspectives, and supports the argument that an interplay of forces and molecular kinetics is at the heart of spindle function (24). Nonetheless, a phenomenological and quantitative understanding of the metaphase spindle is starting to emerge, in part by virtue of great advances in quantitative methods (see **Figure 1**). Polarization microscopy (**Figure 1a**) was one of the first techniques used to visualize the mitotic spindle (50). This simple noninvasive technique has recently provided remarkable insights into the liquid crystal nature of the spindle through the analysis of orientational fluctuations of microtubules (9). Speckle microscopy (**Figure 1b**) is based on the incorporation of fluorescently labeled tubulin dimers in spindle microtubules.

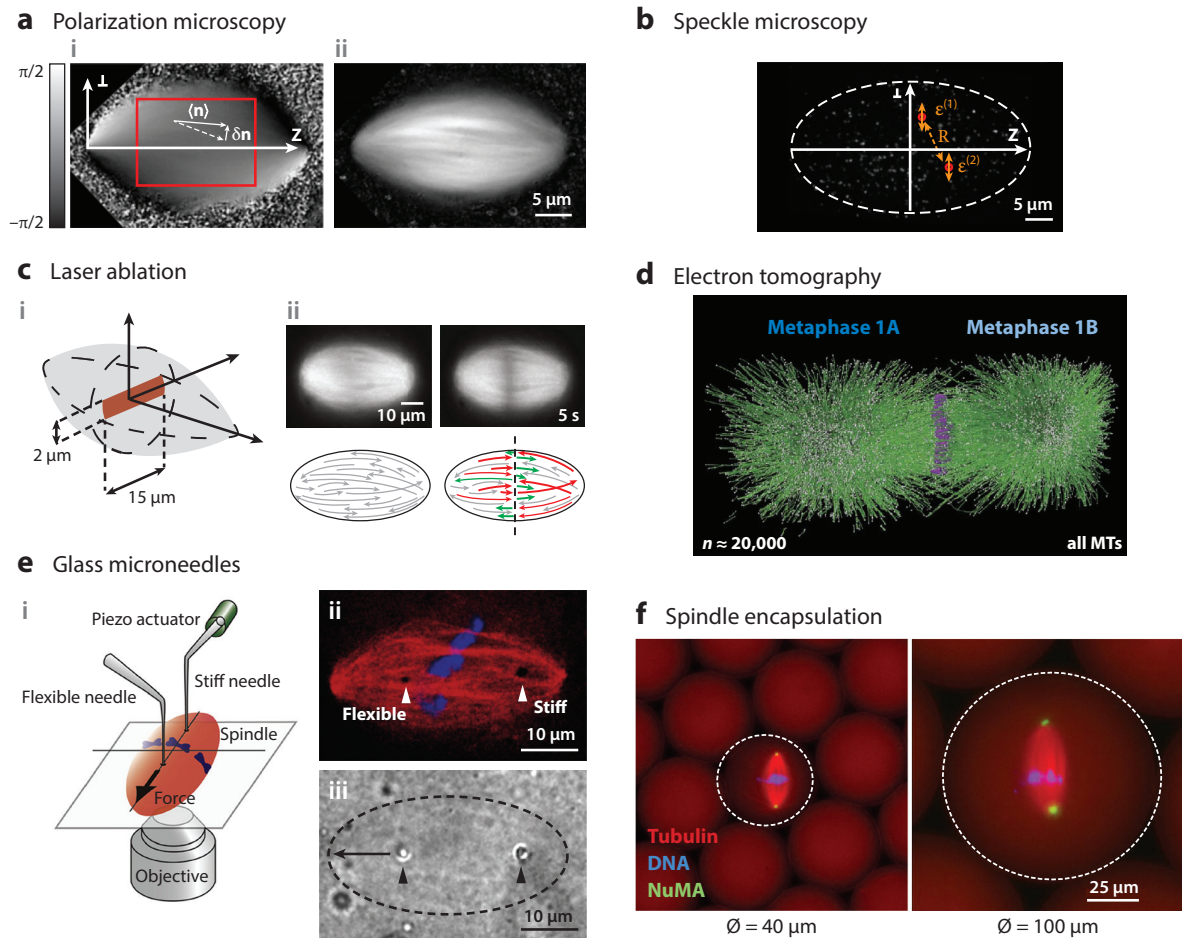


Figure 1

Experimental techniques providing quantitative measurements of the metaphase spindle. (a) Slow orientational angle (i) and retardance (ii) of microtubules in a *Xenopus laevis* meiotic spindle. Adapted from Reference 9. (b) A frame of a single-molecule time-lapse movie of fluorescently labeled tubulin dimers in a *X. laevis* meiotic spindle. Adapted from Reference 9. (c) (i) Geometry of a laser cut in a spindle. (ii) Images of a fluorescently labeled *X. laevis* meiotic spindle (top) and sketch of the microtubule architecture (bottom) before and after the cut. Adapted from Reference 10. (d) Three-dimensional reconstruction of a *Caenorhabditis elegans* metaphase spindle by combining electron tomography and live-cell imaging. Adapted from Reference 98. (e) (i) Experiments using flexible and stiff microneedles to characterize the viscoelastic properties of the metaphase spindle. (ii) Confocal image of a *X. laevis* spindle. Microtubules are indicated in red and chromosomes in blue. (iii) Bright-field image of the same spindle. Arrowheads indicate the tips of the needles, and the arrow indicates the direction of the applied force. Adapted with permission from Reference 108. (f) Encapsulation of *X. laevis* metaphase-arrested egg extract droplets in oil and subsequent formation of spindles. Abbreviation: MT, microtubule. Images adapted with permission from Reference 45.

This technique allows for accurate measurements of microtubule lifetime distributions (88) and two-point microrheology measurements (9), which show that stresses are propagated by the local interactions of microtubules. The polarity and length distribution of microtubules in spindles were recently unveiled by means of the study of synchronous microtubule depolymerization waves triggered by laser ablation (Figure 1c) (10). The combination of electron tomography with live-cell imaging has only very recently provided an accurate three-dimensional reconstruction of

the architecture of large spindles in metazoans (**Figure 1d**) (98). Spindle rheology was studied by means of accurate force measurements using glass microneedles (**Figure 1e**), revealing anisotropic viscoelastic properties of the spindle (108). Finally, spindle encapsulation in cell-like compartments in vitro showed that spindle size can adapt to cytoplasmic volume (**Figure 1f**). Many of these recent quantitative studies of the internal organization, dynamics, and mechanics of spindles were carried out in *Xenopus laevis* egg extracts (21, 44), in which spindles of $\sim 40\ \mu\text{m}$ in length can be assembled in a cell-free environment and can be easily perturbed both physically and chemically. Hence, most of the discussion below is based on experimental evidence from this system.

The structure of this review is as follows: First, we provide an overview of the current state of understanding of microtubule dynamics in spindles and their implications for spindle architecture. Second, we discuss the regulation of spindle size and mass and argue that microtubule nucleation is the key process. Finally, we discuss the role of molecular motors and other microtubule-associated proteins in spindle mechanics and morphology.

2. MICROTUBULE DYNAMICS

Microtubules are polar filaments composed of $\alpha\beta$ -tubulin heterodimers with a fast-growing plus end and a slow-growing minus end (15, 48). Microtubule ends undergo stochastic changes between polymerizing and depolymerizing states (see **Figure 2a,b**), a phenomenon known as dynamic instability (77). Microtubules in the spindle can be divided into three different classes: kinetochore microtubules, nonkinetochore (sometimes referred to as interpolar) microtubules, and astral

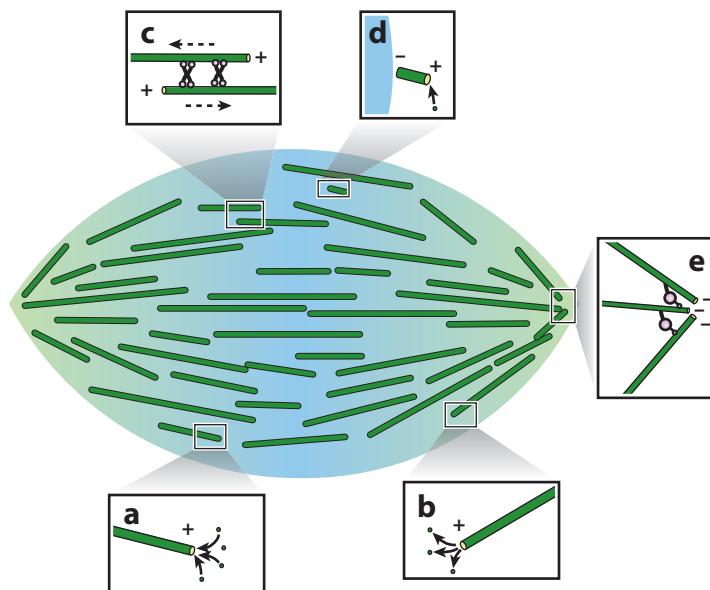


Figure 2

Schematic description of the metaphase spindle, showing some of the most relevant physical processes. Microtubules are depicted in green, and only a small fraction of microtubules are highlighted for illustration purposes. The blue area corresponds to the region where microtubules are nucleated near chromosomes. (a) Microtubule polymerization. (b) Microtubule depolymerization. (c) Antiparallel sliding driven by kinesin-5 motors generates a poleward flux. The dashed arrows indicate microtubule movement. (d) Microtubule nucleation near chromosomes. (e) Minus end clustering driven by dynein motors.

microtubules (30). Kinetochore microtubules, defined to be those with one end embedded in the kinetochore, are crucial for signaling and chromosome positioning in prometaphase and metaphase and are believed to drive chromosome motion in anaphase (117). Some kinetochore microtubules extend from the kinetochore to the centrosome, but many do not span this full distance and instead appear to be cross-linked to nonkinetochore microtubules (25, 71, 98). Extensive evidence demonstrates that kinetochore microtubules are selectively stabilized, but their precise polymerization/depolymerization dynamics remain unclear. It is also not known to what extent kinetochore microtubules are nucleated at centrosomes or kinetochores or result from microtubules not anchored at either of those structures (124). Astral microtubules, defined as those that emanate away from the spindle's poles, position the spindle (128) by either pushing off the cell cortex (35, 118), using cortically anchored pulling forces (27, 40–42, 63), interacting with force generators in the cytoplasm (61, 109), or a combination of all of these processes (127). The remaining microtubules, which are not kinetochore microtubules or astral microtubules, are referred to as nonkinetochore microtubules. These microtubules make up the bulk of microtubules in large spindles in metazoans. In the anastral spindles formed in *X. laevis* egg extract, more than 90% of the microtubules are nonkinetochore microtubules (24, 86). Hereinafter, we refer to nonkinetochore microtubules as simply microtubules and discuss their dynamics.

Microtubules in spindles polymerize at a velocity of $v_p \sim 10\text{--}20 \mu\text{m}/\text{min}$ —as measured by EB1 (end binding 1) protein tracking, which is a polymerization plus end-tracking protein (10, 20, 53, 97, 116)—similar to the speed of polymerizing microtubule plus ends in *Xenopus* egg extracts far removed from spindles (5, 123). Directly measuring microtubule depolymerization in spindles is challenging, as there is no marker for a depolymerizing plus end. Instead, microtubule depolymerization can be measured by triggering synchronous waves of microtubule depolymerization by cutting the spindle structure with a glass needle or a laser (see **Figure 1c**) (10, 20, 116). Upon cutting microtubules, new plus and minus ends are created, and the newly created plus ends depolymerize toward the minus ends. The microtubule depolymerization wave propagates at a velocity of $v_d \sim 35 \mu\text{m}/\text{min}$, corresponding to the microtubule depolymerization velocity. Microtubules undergo transitions between polymerization and depolymerization, termed catastrophes, and the reverse transitions, termed rescues (34). It is not possible to directly measure the statistics of catastrophes and rescues in spindles, because individual microtubules cannot be resolved due to their high density. Instead, the statistics by which individual tubulin molecules incorporate and disincorporate provide related information (88). These measurements reveal that the average lifetime of a microtubule in *Xenopus* egg extract spindles is $\tau \sim 16 \text{ s}$, in agreement with previous measurements of the lifetime of microtubules in *Xenopus* egg extracts far removed from spindles (5, 123). From the polymerization and depolymerization velocities, in combination with the lifetime of a microtubule, one can infer that microtubule lengths are exponentially distributed and that the average microtubule length is $\ell = 2\tau/(v_p^{-1} + v_d^{-1}) \sim 7 \mu\text{m}$ (76). This microtubule length distribution and average length have been independently confirmed by laser ablation (10) (see Section 3). Since the polymerization velocity, lifetime, and lengths of microtubules are the same inside and outside of spindles in *Xenopus* egg extracts, we conclude that the spindle environment does not modify the polymerization/depolymerization dynamics of microtubules. Furthermore, the observations that newly generated microtubule minus ends are stable (10) and that the inferred microtubule plus end dynamics are sufficient to account for tubulin turnover in the spindle (10, 88) support the argument that the dynamic instability of microtubule plus ends accounts for the overwhelming majority of tubulin turnover in the spindle. The relatively short microtubule length and lifetime compared to the length and lifetime of a spindle ($\sim 40 \mu\text{m}$ and up to hours, respectively) confer a highly dynamic nature to spindles, which allows them to recover after damage (116), to fuse (36), and to adapt their size to volume constraints (see **Figure 1f**) (38, 45).

In addition to rapid turnover, microtubules in the spindle constantly slide relative to each other and move toward the spindle poles. This motion results from the activity of kinesin-5, a tetrameric kinesin molecular motor that is able to cross-link and slide antiparallel microtubules, generating a poleward flux in spindles (see **Figure 2c**) (68, 81, 104, 125). The sliding velocity has been measured by photoactivation, speckle microscopy, and single-molecule measurements, resulting in $v_t \sim 2.5 \mu\text{m}/\text{min}$ (10, 119). The continual poleward motion of tubulin in the spindle, termed flux, was originally envisioned to be caused by individual microtubules polymerizing at their plus ends and depolymerizing at their minus ends such that they maintain a constant length as tubulin molecules move through them. While such a mechanism might hold for kinetochore microtubules, it is implausible for nonkinetochore microtubules since it is now realized that they are short compared to the length of the spindle, that their minus ends are stable, and that their motion and turnover are not coupled (88). Thus, the flux of nonkinetochore microtubules is almost certainly caused by these short microtubules sliding relative to each other, as they independently turn over due to the dynamic instability of their plus ends (11, 78). Although not directly proven, the assumption is that microtubules move to the pole to which the minus ends point. This sliding and the highly dynamic nature of microtubules imply that the length of a spindle cannot be explained by the simplest version of the slide-and-cluster model (11), in which microtubules nucleated at the chromosomes are transported all the way to the poles, where they are clustered by dynein. The reason for this is that the flux velocity and lifetime of microtubules result in the displacement of $v_t \tau \sim 1 \mu\text{m}$ before a microtubule disappears. Thus, microtubules in the spindle never move far from where they are nucleated, and if microtubules nucleated only at chromosomes, the length of the spindle would be of the order of the length of an individual microtubule, which is not the case in *Xenopus* egg extract spindles. The implication is thus that the slide-and-cluster model must be supplemented with microtubule nucleation throughout the structure, rather than only at the chromosomes. Additionally, the evidence that microtubule dynamics are the same inside and outside of spindles (88) implies that the enrichment of microtubules in spindles comes from local increased microtubule nucleation around chromosomes. In the next two sections, we discuss how the interplay of microtubule transport and nucleation can account for spindle architecture and size.

3. SPINDLE ARCHITECTURE

The number of microtubules in spindles can range from tens to hundreds of thousands. They are usually in a dense phase, and single microtubules cannot be resolved using light microscopy or even superresolution techniques (105). Femtosecond laser ablation was recently shown to circumvent this problem and to unveil the organization of microtubules in spindles. This technique can be used to study the length distribution and polarity of microtubules throughout spindles (10). The latter can be defined as the fraction of microtubules pointing in one direction in a certain slice perpendicular to the spindle long axis (10). It was found that microtubule lengths are exponentially distributed, with an average length that depends on their position in the spindle as measured from their plus ends: Microtubules are shorter at the poles ($\sim 2 \mu\text{m}$), and their length monotonically increases away from the poles up to $\sim 14 \mu\text{m}$ in the center (see **Figure 3**). A gradient in microtubule polarity was also observed; this gradient was subsequently confirmed by nonlinear optical microscopy (130). Taken together, the evidence indicates that this complex internal organization naturally results from a simple picture in which microtubule polymerization/depolymerization dynamics are spatially uniform and microtubules continuously slide poleward, as described above, in conjunction with nucleation occurring throughout the spindle with a spatially varying rate that is highest in the center of the spindle, near chromosomes (10). While this model explains the internal variations in microtubule lengths and polarity in spindles, a complete understanding of

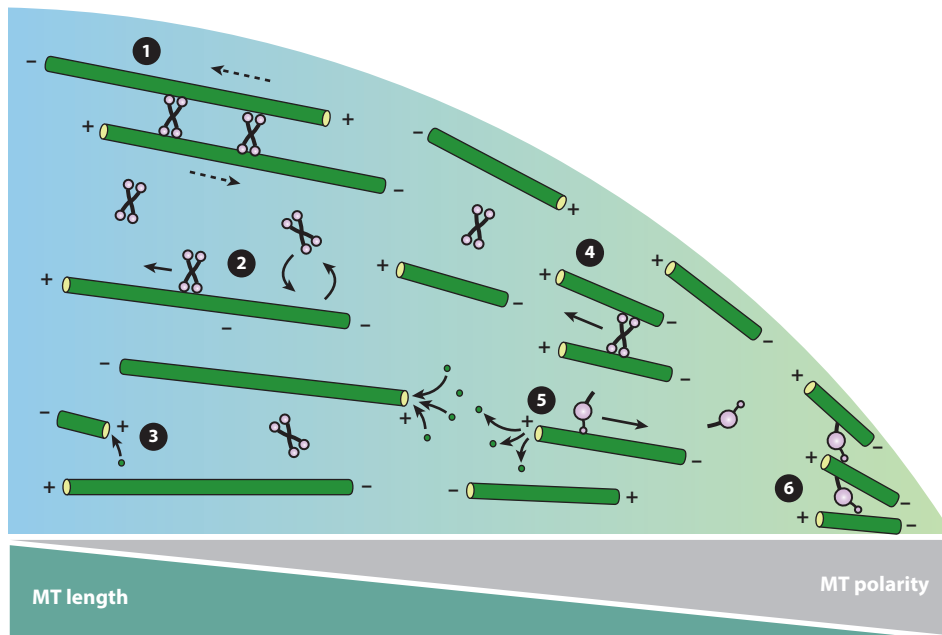


Figure 3

Metaphase spindle architecture in *Xenopus laevis* meiotic spindles. (1) Kinesin-5 motors cross-linking a pair of antiparallel microtubules. In this case, motors do not move, and they drive microtubule sorting. (2) Kinesin-5 motors bind and unbind from microtubules and walk to their plus ends. (3) Microtubule nucleation is not homogeneous in the spindle; rather, it is greater near chromosomes. (4) A kinesin-5 motor cross-linking a pair of parallel microtubules. In this case, the microtubule pair does not move, but the kinesin-5 motor moves to the plus ends. (5) Dynein motors move to the minus ends of microtubules. (6) Dynein motors accumulate at the poles. Dashed arrows indicate microtubule movement, and solid arrows indicate motor movement. The color gradient indicates that the nucleation rate is larger in the spindle midplane and decreases toward the pole. Hence, poleward transport of microtubules due to kinesin-5 leads to longer microtubules at the spindle midplane and shorter microtubules in the poles and to a polarity gradient due to microtubule sorting. Abbreviation: MT, microtubule.

spindle architecture requires incorporating the mechanisms that determine the spatial variation in microtubule nucleation (see Section 4) as well as the mechanisms that determine the alignment of microtubules and the shape of the spindle (see Section 5.2). It is ultimately desirable to have an understanding of the molecular basis of these processes. While kinesin-5 is the primary motor that drives microtubule sliding in the spindle, dynein is thought to be primarily responsible for pole formation (Figure 3) (11, 67, 75, 85). Both kinesin-5 and dynein, despite their very different behaviors and biochemical activities, are enriched at poles (74, 103). While the localization of dynein at spindle poles is naturally explained by its minus end-directed motility, the reason that kinesin-5, a plus end-directed motor, accumulates at poles is less clear. One hypothesis is that dynein drives poleward transport of kinesin-5 to the poles, where it contributes to parallel microtubule cross-linking (119).

The central importance of kinesin-5 and dynein to spindle architecture is clearly revealed by the dramatic effect of inhibiting these motor proteins. Kinesin-5 is essential for bipolar spindle assembly in higher eukaryotes, and its inhibition by means of *S*-trityl-L-cysteine or monastrol (7, 70, 106, 111), or removal (39), leads to the formation of monopolar structures (see Figure 4,

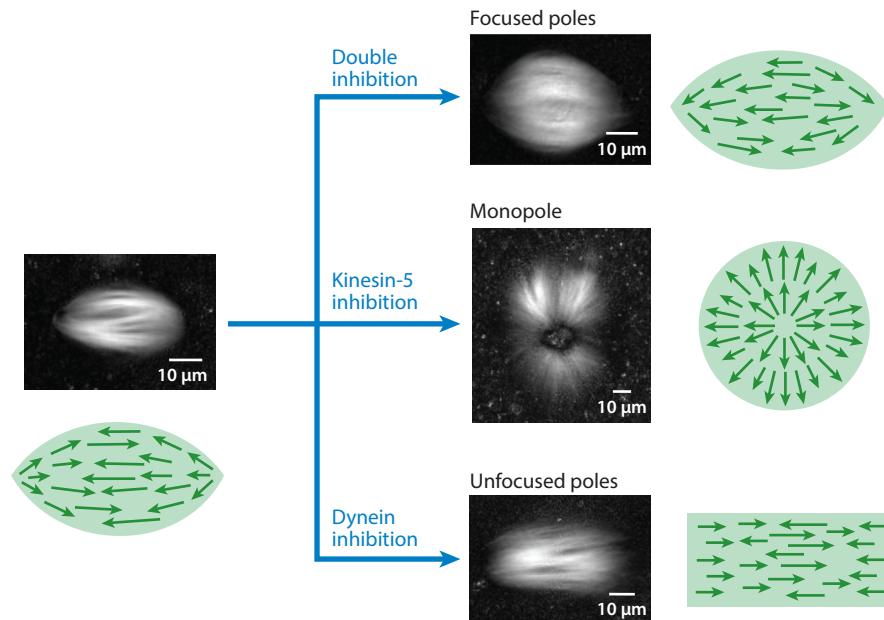


Figure 4

Role of kinesin-5 and dynein in metaphase spindle morphology. In the unperturbed case, the spindle has a bipolar structure, and there is a gradient of polarity along the spindle long axis. In the dynein-inhibited case, the spindle shows a flaglike structure, and the polarity gradient is reinforced. Conversely, in the kinesin-5-inhibited case, the spindle becomes a monopole (or aster), with all the microtubule plus ends pointing outward. Finally, the double inhibition of kinesin-5 and dynein surprisingly leads to a bipolar structure; however, the polarity gradient is lost, in contrast to the unperturbed case. Green arrows indicate the orientation and polarity of microtubules. Spindle images correspond to microtubule retardance using polarization microscopy in *Xenopus laevis* meiotic spindles.

monopole image). This process has been proposed to be driven by dynein minus end clustering (31, 46, 122). Once monopolar structures are assembled, microtubule transport is greatly reduced, with the consequent loss of the polarity gradient found in bipolar spindles. A protein termed monastrol antagonistic compound 1 (MAC1) was recently found to rescue monastrol-treated spindles in cells (1). MAC1 induces the formation of microtubule nucleation centers, allowing kinesin KIF15 to recover bipolarity in the absence of kinesin-5 activity. In monopolar structures, microtubule plus ends point outward, and the polarity profile is constant along the radial direction (20). Conversely, if the dynein-dynactin complex is inhibited by using p50 dynamitin or p150-CC1 (10, 22, 80) or is depleted (83), poles unfocus, and flaglike structures are formed (see **Figure 4**, image showing unfocused poles). In this case, the polarity gradient becomes more pronounced than in normal bipolar spindles (10). Intriguingly, if both motors are inhibited, the spindle maintains its bipolar structure (see **Figure 4**, image showing focused poles) (10, 80), but with a highly perturbed microtubule polarity gradient (10). Thus, while the bipolar structure of the spindle may be determined by the relative balance of kinesin-5 and dynein, the proper internal organization of the spindle evidently depends on the magnitude of their activity.

4. MICROTUBULE NUCLEATION

Next, we discuss the mechanisms underlying spindle size. As mentioned above, the mitotic spindle is a highly dynamic structure in which all the microtubules constituting the structure are renewed

in a few tens of seconds. Such a dynamic process requires constant microtubule nucleation, which is enriched near chromosomes in acentrosomal spindles. How is microtubule nucleation spatially regulated? The assembly of microtubules in *Xenopus* egg extract spindles requires the Ras-related nuclear (Ran) protein pathway (14). Conversion of the GDP-bound form of Ran (RanGDP) to the GTP-bound form of Ran (RanGTP) occurs in the vicinity of chromosomes through the regulator of chromatin condensation 1 (RCC1), whereas RanGTP hydrolysis occurs throughout the cytoplasm due to the Ran-GTPase-activating protein (RanGAP). In this way, a RanGTP gradient is formed around chromosomes. However, the relationship between the length and magnitude of this gradient and spindle size is controversial (14, 91). Factors that regulate microtubule nucleation (SAFs) are sequestered in the cytoplasm by the importin- α -importin- β dimer and are released by RanGTP interacting with importin- β (13, 14, 58). The localization of some of these SAFs strongly depends on the presence of microtubules, leading to the hypothesis that microtubule nucleators are localized by the microtubules that they generate (91). These results are consistent with other evidence arguing for the importance of branching, i.e., microtubules being used as templates for Ran-regulated SAFs to nucleate new microtubules (20, 52, 91, 94). This mechanism has been proposed to ensure the preservation of local microtubule polarity and efficient amplification (94). However, it has been unclear to what extent these processes are sufficient to explain the spatial regulation of microtubule nucleation in the spindle. Recently, laser ablation revealed the spatial distribution of minus ends in microtubule structures, which can be used as a proxy for the sites of microtubule nucleation (20). Such measurements revealed that the microtubule nucleation profile decays monotonously far from chromatin (20). The experimentally measured microtubule density and nucleation profiles were found to be in excellent agreement with a mathematical model based on autocatalytic microtubule nucleation that is spatially regulated by the availability of the active form of SAFs (see Reference 20, **Figure 5**, and sidebar titled Autocatalytic Microtubule Growth). Thus, the regulation of microtubule nucleation appears to be a two-step process: Nucleators are first activated by proximity to chromosomes and then trigger microtubule nucleation, mainly by their association with other microtubules (20). This process generates an autocatalytic wave of microtubule nucleation that is spatially regulated by the gradient of active nucleators from chromosomes. This gradient is also affected by microtubule dynamics because they regulate the nucleator activity by acting as the substrate where active nucleators need to bind to nucleate microtubules. Thus, the relevant length scale for setting the size of spindles is the distance at which a microtubule generates one or fewer microtubules. This mechanism explains the upper limit in spindle size in large cells and in cell-free extracts, where components are virtually unlimited (18, 20, 79). Further work will be required to determine whether this mechanism also contributes to the changes in spindle size over development and to the changes in *in vitro* compartments (see **Figure 1f**) (38).

5. SPINDLE MECHANICS

Chromosome segregation and spindle assembly require the movement and reorganization of microtubules in the spindle. These movements are ultimately driven by mechanical forces generated by motor proteins within the structure. Understanding the mechanics of the spindle requires understanding how and where forces (and torques) are generated and how the spindle responds to such forces (and torques).

The spindle contains a wide variety of microtubule-associated proteins (MAPs). MAPs can be classified as motor or nonmotor, depending on whether they generate force through an ATP cycle or not, respectively. Motor MAPs such as dynein and kinesin are involved in a variety of spindle processes that can affect microtubule polymerization/depolymerization dynamics or produce pulling/pushing forces that transport organelles, slide antiparallel microtubules (**Figure 2c**), and

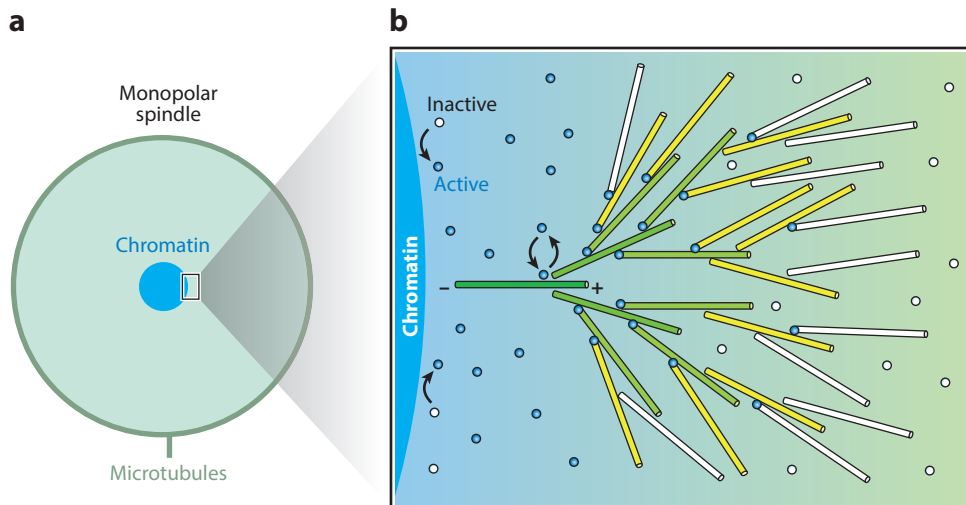


Figure 5

(a) Schematic picture of a monopolar spindle under kinesin-5 inhibition in *Xenopus laevis* egg extract in which microtubules radially nucleate from chromatin. The mass of microtubules is denoted in green, and chromatin is shown in the center in blue. (b) Autocatalytic microtubule nucleation. SAFs are activated close to the chromatin surface by RanGTP (blue circles) and are deactivated elsewhere (white circles). When activated, nucleators can bind along microtubules and nucleate a new microtubule, maintaining the same polarity as the mother microtubule. This autocatalytic process leads to a wave of microtubule growth that is controlled by the spatial gradient of active nucleators extending from chromatin. The different colors of microtubules (dark green, light green, yellow, and white) indicate the different generations of newborn microtubules through the autocatalytic process from the oldest (dark green) to the youngest (white).

focus spindle poles (**Figure 2e**) (17). Nonmotor MAPs influence the stability of microtubule geometries such as asters or bundles (93), move along active microtubule networks through asymmetric friction (29), and generate entropic forces driving antiparallel microtubule sliding (65). Force generation within the spindle is mainly due to microtubule polymerization/depolymerization, motor-based microtubule sliding, and minus end clustering (**Figure 2**) (17, 48, 117). As the spindle is an entangled network of microtubule filaments being simultaneously acted on by diverse motor and nonmotor MAPs, it is exceedingly difficult to develop a realistic, microscopically based description of spindle mechanics. Even if such models could be developed, it would be extremely challenging to experimentally test them. An alternative approach is to develop physically based coarse-grained models that are appropriate for describing larger-length-scale behaviors and that can be directly compared to experiments. We now turn to such continuum coarse-grained descriptions.

5.1. Spindle Rheology

The spindle behaves as a liquid-like material in certain cases, being able to fuse with other spindles (36) or to rearrange its interior after physical perturbations, such as those from microneedles or laser ablation (10, 108, 116). Other experiments showed that the spindle can display more complex mechanical properties, such as viscoelastic mechanics (54, 108, 114), hysteresis under force-compression cycles, and plasticity under large compression forces (54). What are the origins of the viscoelastic nature of the spindle? A viscoelastic material has properties of both fluids and elastic materials. Purely elastic materials are able to store energy when deformed, but they do not

AUTOCATALYTIC MICROTUBULE GROWTH

We consider a simplified one-dimensional model of autocatalytic microtubule nucleation motivated by monopolar spindle growth (see **Figure 5**) (20). We define the microtubule-bound and microtubule-unbound populations of active nucleators (or active SAFs) as $n_b(x, t)$ and $n_u(x, t)$, respectively. When unbound, active nucleators can diffuse with diffusion coefficient D and can become inactive with rate k_0 . Active nucleators can bind to microtubules with rate k_b and can unbind with rate k_u . A bound nucleator can nucleate a microtubule from a preexisting microtubule with rate k_{bra} . Since a daughter microtubule nucleates at a certain distance from the minus end of the mother microtubule, there is a flux of microtubule mass that will advance with a certain velocity. This velocity can be obtained from the following argument: Let us assume that a nucleator can bind anywhere along a microtubule. Since microtubule lengths are exponentially distributed with an average length ℓ , a nucleator will bind at a distance ℓ from the minus end of the mother microtubule. This leads to a mass flux with velocity equal to the polymerization velocity v_p . Finally, we denote the number density of microtubule plus ends as $\rho(x, t)$. Given the previous considerations, the dynamical equations governing the system read

$$\partial_t n_u = D \partial_x^2 n_u - k_b \ell_b n_u \rho + k_u n_b - k_0 n_u, \quad 1.$$

$$\partial_t n_b = k_b \ell_b n_u \rho - k_u n_b, \quad 2.$$

$$\partial_t \rho = -v_p \partial_x \rho + k_{bra} n_b - \Theta \rho, \quad 3.$$

where ℓ_b is a characteristic binding length scale for the active nucleators and Θ is the average microtubule turnover rate. Unbound nucleators are assumed to be activated with constant rate Γ at the chromatin surface in the center of the monopole ($x = 0$) (see **Figure 5b**). This leads to a boundary condition for the flux of active nucleators at the chromatin surface; the condition is expressed as $-D \partial_x n_u|_{x=0} = \Gamma$. At steady state, Equation 2 leads to $n_b(x) = \ell_0 n_u(x) \rho(x)$, where $\ell_0 \equiv \ell_b k_b / k_u$. Using the last expression in Equation 1 and the boundary condition at $x = 0$, we obtain the profile of unbound active nucleators at steady state:

$$n_u(x) = A e^{-x/\ell_u}, \quad 4.$$

where $A = \Gamma / \sqrt{D k_0}$ is the amplitude of the gradient, proportional to the rate of activation Γ at the chromatin surface, and $\ell_u \equiv \sqrt{D/k_0}$ is the characteristic length scale of the gradient of unbound active nucleators. Finally, by using Equation 3 we find the steady-state distribution of microtubule plus ends:

$$\rho(x) = \lambda(x) e^{-x/\ell}, \quad 5.$$

where $\lambda(x) = \rho(0) \exp[\alpha(1 - e^{-x/\ell_u})]$ is a lifetime-independent function, $\rho(0)$ is the density of plus ends at $x = 0$, and $\alpha \equiv \frac{\Gamma \ell_0 k_{bra}}{v_p k_0}$ is a dimensionless parameter. Hence, we have two main length scales in the system: ℓ_u , which is dictated by the gradient of unbound active nucleators and does not depend on microtubule lifetime, and ℓ , which is the mean microtubule length and does depend on microtubule lifetime.

dissipate energy when load is applied. An ideal spring is the prototypical example of an elastic object. Conversely, fluids dissipate energy under load due to viscous friction, as in the case of a dashpot. A viscoelastic material combines both properties: It is able to store energy and also dissipates energy. Simple mathematical models of viscoelastic materials can be built by using the combination of springs and dashpots. Many elements, such as kinetochore microtubules, nonkinetochore microtubules, motor proteins, and passive cross-linkers, could confer elasticity to the spindle (17, 108, 117). The boundary of the spindle can give rise to an apparent elasticity due to surface tension or active contractile stresses, even if the spindle is entirely viscous, similar to how

a droplet of water elastically resumes a spherical shape after being perturbed, even though water is a purely viscous material. In turn, microtubules and motor proteins can actively generate ~ 1 – 10 -pN forces by hydrolyzing GTP (23, 64) or ATP (37, 55, 120), respectively. Microtubule turnover occurs in ~ 5 min for kinetochore microtubules and in ~ 10 s for nonkinetochore microtubules, whereas motor protein stepping is ~ 10 ms, and the binding/unbinding timescale is ~ 0.1 – 1 s (48). This implies a great variety of processes acting on several different timescales (108). The fact that cross-linkers in the entangled spindle network have their own binding/unbinding kinetics leads to a fluidization process at long timescales (82, 92, 108, 115), resulting in an apparent viscosity of the spindle of $\sim 10^2$ Pa·s (108), which is at least a hundred times larger than the one measured in the cytoplasm by studying the Brownian motion of cytoplasmic particles near spindles (2). The apparent viscosity is proportional to the elastic modulus of the network and is inversely proportional to the typical rate of the cross-linker kinetics (57, 95). With an elastic modulus on the order of kilopascals (54), we find the typical cross-linking timescale to be ~ 0.1 s, in agreement with typical motor binding/unbinding kinetics (48). A key property of the spindle is that it is anisotropic, with the majority of microtubules oriented along its long axis. This property has direct consequences for the spindle's mechanical properties, leading to greatly distinct elastic and viscous properties between the long and short axes (54, 108, 114). The Young's modulus along the long axis has been found to be on the order of several kilopascals, whereas along the short axis it is estimated to be tenfold lower (54). These values are still several orders of magnitude greater than the Young's modulus measured in in vitro cytoskeletal networks (2–10 Pa) (121), reflecting the distinct properties of the spindle relative to simple entangled cytoskeletal networks.

Micromechanic experiments using microneedles on *X. laevis* meiotic spindles have shown that the simplest viscoelastic model consistent with the short-axis rheology of the spindle is a Zener-type model (108, 114). This is the simplest model that describes creep and stress relaxation (16). The model is based on a dashpot and a spring in series. The model predicts an elastic behavior at short timescales (< 1 – 10 s) and long timescales (> 100 s), while at intermediate timescales (~ 10 – 100 s) it exhibits a fluid-like behaviour. One study found that a Zener-type model described the mechanics of the long axis of the spindle (114), while another work suggested that this response is purely fluid (108). An important difference between the two studies is that in the first case the two microneedles interacted with the poles and in the second case only a stiff microneedle interacted with a pole, whereas the other flexible microneedle remained in the spindle center. Hence, the differences in the mechanical behavior along the long axis may be attributed to spatially dependent rheological properties. These differences could arise directly from the nonhomogeneous distribution of bound motor proteins cross-linking the microtubules in the spindle. Nonkinetochore microtubules seem to be responsible for the viscoelastic response at short timescales (108). In contrast, at long timescales (~ 5 min), kinetochore microtubules were suggested to be the relevant elastic elements. At intermediate timescales, the viscous regime dominates, and the origin of the apparent friction drag is suggested to be due to the dynamic cross-linking of microtubules (108). However, spindles can last for hours, and the rheological studies were done on a timescale of minutes. The spindle should behave as a fluid at sufficiently long times due to the turnover of microtubules and MAPs. Further studies must be done to clearly resolve these issues.

5.2. The Spindle as an Active Liquid Crystal

The previous studies focus on the rheological properties of the spindle as a complex material; however, the spindle is an out-of-equilibrium structure that constantly consumes ATP and GTP and can generate stresses on its own. Hence, it is an active system (9, 56, 57, 69, 95).

Continuum active hydrodynamic theories are emerging as powerful predictive tools to understand problems in molecular cell biology at the coarse-grained level (69, 95). Such theories are based on symmetry arguments and/or on the formalism of linear irreversible thermodynamics (69). To provide a top-down approach, one first needs to identify the relevant physical fields describing the spindle. The simplest choice is to define coarse-grained fields describing the orientation, polarity, and concentration of microtubules. We recently used the intimate connection between the statistics of spatiotemporal correlation functions of the spontaneous fluctuations of microtubule density, orientation, and stress and the underlying physical processes that drive them. This approach showed that spindles behave as continuum materials whose properties can be understood in the framework of an active liquid crystal description (9). A general hydrodynamic limit description that is consistent with spatiotemporal correlations of microtubule density, orientation, and microrheology (9) is detailed in the sidebar titled Active Liquid Crystal Description of the Metaphase Spindle; this description includes the dynamics of microtubule concentration and orientation and the different types of passive and active stresses. A hallmark of active polar gels such as the cytoskeleton is the presence of active stresses due to the self-organized action of molecular motors and polar filaments. The latter can be extensile or contractile, depending on the nature of the system (69). Examples of contractile behavior are found in actomyosin systems (3, 84, 113) and microtubule networks in cytoplasmic extracts (6, 31, 126). In contrast, extensile stresses can arise due to polarity sorting, leading to active flows in microtubule bundles in vitro (43, 101). The combination of plus end- and minus end-directed multimeric motor populations in vitro can lead to the formation of complex, out-of-equilibrium steady-state structures, such as asters, vortices, and networks of interconnected poles (112).

Active stresses can have, in general, an isotropic part that acts like a pressure and an anisotropic part, an intrinsically nonequilibrium phenomenon that can give rise to steady-state flows (87) (see sidebar titled Active Liquid Crystal Description of the Metaphase Spindle). The dynein-dependent bulk contraction of taxol-stabilized microtubule networks in *Xenopus* egg extracts suggests that dynein drives contractile stress in the spindle through minus end clustering (31). This dynein-mediated isotropic active stress was estimated to be $\simeq 4$ Pa, which accounted for at least $\simeq 96\%$ of contractile stresses present in those microtubule networks (31). Isotropic contractile stress generated by dynein may explain dynein's role in spindle pole formation. Measurements of stress fluctuations in the spindle also revealed the presence of an anisotropic active stress of $\simeq 70$ Pa (9) (see sidebar titled Active Liquid Crystal Description of the Metaphase Spindle) (9). In contrast, the role of kinesin-5 in active stress generation is still not understood. Kinesin-5 may not generate appreciable active stresses and may instead function by sliding or actively orienting microtubules.

6. OUTLOOK

Obtaining a complete understanding of the spindle will require establishing how perturbing proteins influences the parameters that characterize the coarse-grained active liquid crystal theory of the spindle, as well as testing whether these changes in parameters are sufficient to account for the resulting changes in spindle architecture and dynamics. Many of these parameters can be measured by studying the internal fluctuations of the relevant fields in spindles (9). However, it would be highly desirable to have theories to relate the microscopic behaviors of microtubules, motors, and other MAPs to the phenomenological coefficients in continuum hydrodynamic descriptions of the cytoskeleton. Despite some progress in this regard (31–33, 66, 69, 107), future work still needs to be undertaken to fully understand the complexity of spindles.

ACTIVE LIQUID CRYSTAL DESCRIPTION OF THE METAPHASE SPINDLE

At a coarse-grained level, we can build local fields that change smoothly over the characteristic timescales and length scales of a system. For example, in a certain region of the spindle, one can average microtubule orientation locally and build a nematic vectorial quantity $\mathbf{n}(\mathbf{x}, t)$ at position \mathbf{x} at time t . Likewise, the polarity strength and microtubule density can also be described as coarse-grained fields $p(\mathbf{x}, t)$ and $c(\mathbf{x}, t)$, respectively. The dynamic equations for such fields are usually of phenomenological origin making use of symmetry arguments (9, 19, 69). To lowest order in the relevant fields:

$$\frac{Dn_\alpha}{Dt} = -v_1 v_{\alpha\beta} n_\beta + \frac{h_\alpha}{\gamma_1}, \quad 6.$$

$$\frac{Dp}{Dt} = \lambda_1 p_\beta \partial_\beta p + \xi n_\beta \partial_\beta c + p(\chi - v p^2) + K_p \nabla^2 p, \quad 7.$$

$$\frac{Dc}{Dt} = -\partial_\beta [c p_\beta v_0 - D \partial_\beta c] + \Gamma - \Theta c, \quad 8.$$

where $h_\alpha = -\frac{\delta F_p}{\delta n_\alpha}$; F_p is the free energy due to nematic distortions; $\delta/\delta n_\alpha$ is the functional derivative with respect to the director \mathbf{n} ; \mathbf{v} is the velocity field; $\frac{Dn_\alpha}{Dt} \equiv \partial_t n_\alpha + v_\beta \partial_\beta n_\alpha + \omega_{\alpha\beta} n_\beta$ is the comoving and corotational derivative of the nematic director orientation; and $\omega_{\alpha\beta} \equiv \frac{1}{2}(\partial_\alpha v_\beta - \partial_\beta v_\alpha)$ and $v_{\alpha\beta} \equiv \frac{1}{2}(\partial_\alpha v_\beta + \partial_\beta v_\alpha)$ are the antisymmetric and symmetric parts of the velocity gradient tensor, respectively. $\frac{Dp}{Dt} \equiv \partial_t p + v_\beta \partial_\beta p$ is the material derivative for the polar field. Here we used $\partial_\alpha \equiv \partial/\partial x_\alpha$ and the Einstein summation convention. The first term in Equation 6 stands for flow alignment of microtubules, while the last terms in Equations 6 and 7 come from the energetic cost of spatial inhomogeneous deformations of the polarity field (19, 69). In Equation 7, the first term introduces self-advection, the second term is a contribution of polarity sorting driven by kinesin-5, and the third term indicates a possible spontaneous polarity due to microtubule branching. $\frac{Dc}{Dt} \equiv \partial_t c + v_\beta \partial_\beta c$ is the material derivative of the concentration field; the first two terms account for self-advection with velocity v_0 and diffusion with coefficient D , respectively; the third term corresponds to microtubule nucleation with rate Γ ; and the last term denotes microtubule catastrophes with constant rate Θ . Finally, force balance in the limit of small Reynolds number reads $\partial_\beta \sigma_{\alpha\beta} = 0$, where $\sigma_{\alpha\beta} = \sigma_{\alpha\beta}^r + \sigma_{\alpha\beta}^a + \sigma_{\alpha\beta}^d$ is the total stress tensor which has passive reactive (r), active (a), and dissipative (d) contributions. The passive reactive contribution is in general a combination of the Ericksen stress and the tensor $h_\alpha n_\beta$ (19). The dissipative and active contributions can be expressed as

$$\sigma_{\alpha\beta}^d = 2 \int_{-\infty}^t dt' G_{\alpha\beta\gamma\nu}(t-t') v_{\gamma\nu}, \quad 9.$$

$$\sigma_{\alpha\beta}^a = W_i(c) \delta_{\alpha\beta} + W(c) q_{\alpha\beta}, \quad 10.$$

where $G_{\alpha\beta\gamma\nu}$ is a general relaxation function describing the anisotropic viscoelastic response of the system and $q_{\alpha\beta} = p_\alpha p_\beta - \frac{p^2}{3} \delta_{\alpha\beta}$ is the nematic order tensor. The active stress contains an isotropic part (W_i) presumably driven by dynein minus end clustering, which has been proposed to have a quadratic form on the microtubule concentration (31), and a traceless part (W), which would be proportional to the microtubule concentration [i.e., $W(c) \propto c$] motivated by studies in ordered suspensions of self-propelled particles (110).

DISCLOSURE STATEMENT

The authors are not aware of any affiliations, memberships, funding, or financial holdings that might be perceived as affecting the objectivity of this review.

ACKNOWLEDGMENTS

We thank K. Ishihara for valuable comments on the manuscript. J.B. acknowledges the support of the Human Frontier Science Program, and D.O. acknowledges the support of the European Molecular Biology Organization.

LITERATURE CITED

1. Al-Obaidi N, Mitchison TJ, Crews CM, Mayer TU. 2016. Identification of MAC1: a small molecule that rescues spindle bipolarity in monastrol-treated cells. *ACS Chem. Biol.* 11:1544–51
2. Alexander SP, Rieder CL. 1991. Chromosome motion during attachment to the vertebrate spindle: initial saltatory-like behaviour of chromosomes and quantitative analysis of force production by nascent kinetochore fibers. *J. Cell Biol.* 113:805–15
3. Alvarado J, Sheinman M, Sharma A, MacKintosh FC, Koenderink GH. 2013. Molecular motors robustly drive active gels to a critically connected state. *Nat. Phys.* 9:591–97
4. Ault JG, Nicklas RB. 1989. Tension, microtubule rearrangements, and the proper distribution of chromosomes in mitosis. *Chromosoma* 98:33–39
5. Belmont LD, Hyman AA, Sawin KE, Mitchison TJ. 1990. Real-time visualization of cell cycle-dependent changes in microtubule dynamics in cytoplasmic extracts. *Cell* 62:579–89
6. Bendix PM, Koenderink GH, Cuvelier D, Dogic Z, Koeleman BN, et al. 2008. A quantitative analysis of contractility in active cytoskeletal protein networks. *Biophys. J.* 94:3126–36
7. Blangy A, Lane HA, d'Hérin P, Harper M, Kress M, Nigg EA. 1995. Phosphorylation by p34^{cdc2} regulates spindle association of human Eg5, a kinesin-related motor essential for bipolar spindle formation in vivo. *Cell* 83:1159–69
8. Borisy GG, Taylor EW. 1967. The mechanism of action of colchicine. *J. Cell Biol.* 34:525–33
9. Brugués J, Needleman DJ. 2014. Physical basis of spindle self-organization. *PNAS* 111:18496–500
10. Brugués J, Nuzzo V, Mazur E, Needleman DJ. 2012. Nucleation and transport organize microtubules in metaphase spindles. *Cell* 149:554–64
11. Burbank KS, Mitchison TJ, Fisher DS. 2007. Slide-and-cluster models for spindle assembly. *Curr. Biol.* 17:1373–83
12. Carpenter AT. 1991. Distributive segregation: motors in the polar wind? *Cell* 64:885–90
13. Caudron M, Bunt G, Bastiaens P, Karsenti E. 2005. Spatial coordination of spindle assembly by chromosome-mediated signaling gradients. *Science* 309:1373–76
14. Clarke PR, Zhang C. 2008. Spatial and temporal coordination of mitosis by Ran GTPase. *Nat. Rev. Mol. Cell Biol.* 9:464–77
15. Conde C, Cáceres A. 2009. Microtubule assembly, organization and dynamics in axons and dendrites. *Nat. Rev. Neurosci.* 10:319–32
16. Creus GJ. 1986. *Viscoelasticity: Basic Theory and Applications to Concrete Structures*. Berlin: Springer-Verlag
17. Cross RA, McAinsh A. 2014. Prime movers: the mechanochemistry of mitotic kinesins. *Nat. Rev. Mol. Cell Biol.* 15:257–71
18. Crowder ME, Strzelecka M, Wilbur JD, Good MC, von Dassow G, Heald R. 2015. A comparative analysis of spindle morphometrics across metazoans. *Curr. Biol.* 25:1542–50
19. de Gennes PG, Prost J. 1974. *The Physics of Liquid Crystals*. Oxford, UK: Clarendon Press
20. Decker F, Oriola D, Dalton B, Brugués J. 2018. Autocatalytic microtubule nucleation determines the mass and size of spindles. *eLife* 7:e31149
21. Desai A, Murray A, Mitchison TJ, Walczak CE. 1998. The use of *Xenopus* egg extracts to study mitotic spindle assembly and function in vitro. *Methods Cell Biol.* 61:385–412
22. Dinarina A, Pugieux C, Corral MM, Loose M, Spatz J, et al. 2009. Chromatin shapes the mitotic spindle. *Cell* 138:502–13
23. Dogterom M, Yurke B. 1997. Measurement of the force-velocity relation for growing microtubules. *Science* 278:856–60
24. Dumont S, Mitchison TJ. 2009. Force and length in the mitotic spindle. *Curr. Biol.* 19:R749–61

25. Elting MW, Prakash M, Udy DB, Dumont S. 2017. Mapping load-bearing in the mammalian spindle reveals local kinetochore fiber anchorage that provides mechanical isolation and redundancy. *Curr. Biol.* 27:2112–22
26. Enos AP, Morris NR. 1990. Mutation of a gene that encodes a kinesin-like protein blocks nuclear division in *A. nidulans*. *Cell* 60:1019–27
27. Fink G, Schuchardt I, Colombelli J, Stelzer E, Steinberg G. 2006. Dynein-mediated pulling forces drive rapid mitotic spindle elongation in *Ustilago maydis*. *EMBO J.* 25:4897–908
28. Flemming W. 1882. *Zellsubstanz, Kern und Zelltheilung*. Leipzig, Ger.: FCW Vogel
29. Forth S, Hsia KC, Shimamoto Y, Kapoor TM. 2014. Asymmetric friction of nonmotor maps can lead to their directional motion in active microtubule networks. *Cell* 157:420–32
30. Forth S, Kapoor TM. 2017. The mechanics of microtubule networks in cell division. *J. Cell Biol.* 216:1525–31
31. Foster PJ, Fürthauer S, Shelley MJ, Needleman DJ. 2015. Active contraction of microtubule networks. *eLife* 4:e10837
32. Gao T, Betterton MD, Jhang AS, Shelley MJ. 2017. Analytical structure, dynamics, and coarse graining of a kinetic model of an active fluid. *Phys. Rev. Fluids* 2:093302
33. Gao T, Blackwell R, Glaser MA, Betterton MD, Shelley MJ. 2015. Multiscale polar theory of microtubule and motor-protein assemblies. *Phys. Rev. Lett.* 114:048101
34. Gardner MK, Zanic M, Howard J. 2013. Microtubule catastrophe and rescue. *Curr. Opin. Cell Biol.* 25:14–22
35. Garzon-Coral C, Fantana HA, Howard J. 2016. A force-generating machinery maintains the spindle at the cell center during mitosis. *Science* 352:1124–27
36. Gatlin JC, Matov A, Groen AC, Needleman DJ, Maresca TJ, et al. 2009. Spindle fusion requires dynein-mediated sliding of oppositely oriented microtubules. *Curr. Biol.* 19:287–96
37. Gennerich A, Carter AP, Reck-Peterson SL, Vale RD. 2007. Force-induced bidirectional stepping of cytoplasmic dynein. *Cell* 131:952–65
38. Good MC, Vahey MD, Skandarajah A, Fletcher DA, Heald R. 2013. Cytoplasmic volume modulates spindle size during embryogenesis. *Science* 342:856–60
39. Goshima G, Vale RD. 2003. The roles of microtubule-based motor proteins in mitosis: comprehensive RNAi analysis in the *Drosophila* S2 cell line. *J. Cell Biol.* 162:1003–16
40. Grill SW, Gönczy P, Stelzer EHK, Hyman AA. 2001. Polarity controls forces governing asymmetric spindle positioning in the *Caenorhabditis elegans* embryo. *Nature* 409:630–33
41. Grill SW, Howard J, Schäffer E, Stelzer EHK, Hyman AA. 2003. The distribution of active force generators controls mitotic spindle position. *Science* 301:518–21
42. Grill SW, Hyman AA. 2005. Spindle positioning by cortical pulling forces. *Dev. Cell* 8:461–65
43. Guillamat P, Ignés-Mullol J, Sagués F. 2016. Control of active liquid crystals with a magnetic field. *PNAS* 113:5498–502
44. Hannak E, Heald R. 2006. Investigating mitotic spindle assembly and function in vitro using *Xenopus laevis* egg extracts. *Nat. Protoc.* 1:2305–14
45. Hazel J, Krutkramelis K, Mooney P, Tomschik M, Gerow K, et al. 2013. Changes in cytoplasmic volume are sufficient to drive spindle scaling. *Science* 342:853–56
46. Heald R, Tournebize R, Blank T, Sandaltzopoulos R, Becker P, et al. 1996. Self-organization of microtubules into bipolar spindles around artificial chromosomes in *Xenopus* egg extracts. *Nature* 382:420–25
47. Hepler PK, Jackson WT. 1968. Microtubules and early stages of cell-plate formation in the endosperm of *Haemantbus katberinae* baker. *J. Cell Biol.* 38:437–46
48. Howard J. 2001. *Mechanics of Motor Proteins and the Cytoskeleton*. Sunderland, MA: Sinauer Assoc.
49. Huxley H, Hanson J. 1954. Changes in the cross-striations of muscle during contraction and stretch and their structural interpretation. *Nature* 173:973–76
50. Inoué S. 1953. Polarization optical studies of the mitotic spindle. I. The demonstration of spindle fibers in living cells. *Chromosoma* 5:487–500
51. Inoué S, Sato H. 1967. Cell motility by labile association of molecules: the nature of the mitotic spindle fibers and their role in chromosome movement. *J. Gen. Physiol.* 50:259–92

52. Ishihara K, Korolev KS, Mitchison TJ. 2016. Physical basis of large microtubule aster growth. *eLife* 5:e19145
53. Ishihara K, Nguyen PA, Groen AC, Field CM, Mitchison TJ. 2014. Microtubule nucleation remote from centrosomes may explain how asters span large cells. *PNAS* 111:17715–22
54. Itabashi T, Takagi J, Shimamoto Y, Onoe H, Kuwana K, et al. 2009. Probing the mechanical architecture of the vertebrate meiotic spindle. *Nat. Meth.* 6:167–72
55. Jannasch A, Bormuth V, Storch M, Howard J, Schäffer E. 2013. Kinesin-8 is a low-force motor protein with a weakly bound slip state. *Biophys. J.* 104:2456–64
56. Joanny JF, Jülicher F, Kruse K, Prost J. 2007. Hydrodynamic theory for multicomponent active gels. *New J. Phys.* 9:422
57. Jülicher F, Kruse K, Prost J, Joanny JF. 2007. Active behaviour of the cytoskeleton. *Phys. Rep.* 449:3–28
58. Káláb P, Pralle A, Isacoff EY, Heald R, Weis K. 2006. Analysis of a RanGTP-regulated gradient in mitotic somatic cells. *Nature* 440:697–701
59. Karsenti E. 2008. Self-organization in cell biology: a brief history. *Nat. Rev. Mol. Cell Biol.* 9:255–62
60. Kashina AS, Baskin RJ, Cole DG, Wedaman KP, Saxton WM, Scholey JM. 1996. A bipolar kinesin. *Nature* 379:270–72
61. Kimura K, Kimura A. 2011. Intracellular organelles mediate cytoplasmic pulling force for centrosome centration in the *Caenorhabditis elegans* early embryo. *PNAS* 108:137–42
62. Kittler R, Pelletier L, Heninger AK, Slabicki M, Theis M, et al. 2007. Genome-scale RNAi profiling of cell division in human tissue culture cells. *Nat. Cell Biol.* 9:1401–12
63. Kiyomitsu T, Cheeseman IM. 2013. Cortical dynein and asymmetric membrane elongation coordinately position the spindle in anaphase. *Cell* 154:391–402
64. Laan L, Husson J, Munteanu EL, Kerssemakers JWJ, Dogterom M. 2008. Force-generation and dynamic instability of microtubule bundles. *PNAS* 105:8920–25
65. Lansky Z, Braun M, Lüdecke A, Schlierf M, ten Wolde PR, et al. 2015. Diffusible crosslinkers generate directed forces in microtubule networks. *Cell* 160:1159–68
66. Liverpool TB, Marchetti MC. 2006. Rheology of active filament solutions. *Phys. Rev. Lett.* 97:268101
67. Loughlin R, Heald R, Nédélec F. 2010. A computational model predicts *Xenopus* meiotic spindle organization. *J. Cell Biol.* 191:1239–49
68. Maddox P, Desai A, Oegema K, Mitchison TJ, Salmon ED. 2002. Poleward microtubule flux is a major component of spindle dynamics and anaphase A in mitotic *Drosophila* embryos. *Curr. Biol.* 12:1670–74
69. Marchetti MC, Joanny JF, Ramaswamy S, Liverpool TB, Prost J, et al. 2013. Hydrodynamics of soft active matter. *Rev. Mod. Phys.* 85:1143–89
70. Mayer TU, Kapoor TM, Haggarty SJ, King RW, Schreiber SL, Mitchison TJ. 1999. Small molecule inhibitor of mitotic spindle bipolarity identified in a phenotype-based screen. *Science* 286:971–74
71. McDonald KL, O'Toole ET, Mastronade DN, McIntosh JR. 1992. Kinetochore microtubules in PTK cells. *J. Cell Biol.* 118:369–83
72. McIntosh JR, Hepler PK, Van Wie DG. 1969. Model for mitosis. *Nature* 224:659–63
73. Meluh PB, Rose MD. 1990. *KAR3*, a kinesin-related gene required for yeast nuclear fusion. *Cell* 60:1029–41
74. Merdes A, Heald R, Samejima K, Earnshaw WC, Cleveland DW. 2000. Formation of spindle poles by dynein/dynactin-dependent transport of Numa. *J. Cell Biol.* 149:851–62
75. Merdes A, Ramyar K, Vechio JD, Cleveland DW. 1996. A complex of Numa and cytoplasmic dynein is essential for mitotic spindle assembly. *Cell* 87:447–58
76. Mirny L, Needleman DJ. 2010. Quantitative characterization of filament dynamics by single-molecule lifetime measurements. *Meth. Cell Biol.* 95:583–600
77. Mitchison T, Kirschner MW. 1984. Dynamic instability of microtubule growth. *Nature* 312:237–42
78. Mitchison TJ. 2005. Mechanism and function of poleward flux in *Xenopus* extract meiotic spindles. *Philos. Trans. R. Soc. B Biol. Sci.* 360:623–29
79. Mitchison TJ, Ishihara K, Nguyen P, Wühr M. 2015. Size scaling of microtubule assemblies in early *Xenopus* embryos. *Cold Spring Harb. Perspect. Biol.* 7:a019182

80. Mitchison TJ, Maddox P, Gaetz J, Groen A, Shirasu M, et al. 2005. Roles of polymerization dynamics, opposed motors, and a tensile element in governing the length of *Xenopus* extract meiotic spindles. *Mol. Biol. Cell* 16:3064–76
81. Miyamoto DT, Perlman ZE, Burbank KS, Groen AC, Mitchison TJ. 2004. The kinesin Eg5 drives poleward microtubule flux in *Xenopus laevis* egg extract spindles. *J. Cell Biol.* 167:813–18
82. Mogilner A, Craig E. 2010. Towards a quantitative understanding of mitotic spindle assembly and mechanics. *J. Cell Sci.* 123:3435–45
83. Morales-Mulia S, Scholey JM. 2005. Spindle pole organization in *Drosophila* S2 cells by dynein, *Abnormal Spindle* protein (Asp), and KLP10A. *Mol. Biol. Cell* 16:3176–86
84. Murrell MP, Gardel ML. 2012. F-actin buckling coordinates contractility and severing in a biomimetic actomyosin cortex. *PNAS* 109:20820–25
85. Nédélec F. 2002. Computer simulations reveal motor properties generating stable antiparallel microtubule interactions. *J. Cell Biol.* 158:1005–15
86. Nédélec F, Surrey T, Karsenti E. 2003. Self-organisation and force in the microtubule cytoskeleton. *Curr. Opin. Cell Biol.* 15:118–24
87. Needleman D, Dogic Z. 2017. Active matter at the interface between materials science and cell biology. *Nat. Rev. Mater.* 2:17048
88. Needleman DJ, Groen AC, Ohi R, Maresca T, Mirny L, Mitchison TJ. 2010. Fast microtubule dynamics in meiotic spindles measured by single molecule imaging: evidence that the spindle environment does not stabilize microtubules. *Mol. Biol. Cell* 21:323–33
89. Nicklas RB. 1983. Measurements of the force produced by the mitotic spindle in anaphase. *J. Cell Biol.* 97:542–48
90. Nicklas RB. 1988. The forces that move chromosomes in mitosis. *Annu. Rev. Biophys. Biophys. Chem.* 17:431–49
91. Oh D, Yu CH, Needleman DJ. 2016. Spatial organization of the Ran pathway by microtubules in mitosis. *PNAS* 113:8729–34
92. Oriola D, Alert R, Casademunt J. 2017. Fluidization and active thinning by molecular kinetics in active gels. *Phys. Rev. Lett.* 118:088002
93. Peterman EJJ, Scholey JM. 2009. Mitotic microtubule crosslinkers: insights from mechanistic studies. *Curr. Biol.* 19:R1089–94
94. Petry S, Groen AC, Ishihara K, Mitchison TJ, Vale RD. 2013. Branching microtubule nucleation in *Xenopus* egg extracts mediated by Augmin and TPX2. *Cell* 152:768–77
95. Prost J, Jülicher F, Joanny JF. 2015. Active gel physics. *Nat. Phys.* 11:111–17
96. Rath O, Kozielski F. 2012. Kinesins and cancer. *Nat. Rev. Cancer* 12:527–39
97. Reber SB, Baumgart J, Widlund PO, Pozniakovskiy A, Howard J, et al. 2013. XMAP215 activity sets spindle length by controlling the total mass of spindle microtubules. *Nat. Cell Biol.* 15:1116–22
98. Redemann S, Baumgart J, Lindow N, Shelley MJ, Nazockdast E, et al. 2017. *C. elegans* chromosomes connect to centrosomes by anchoring into the spindle network. *Nat. Commun.* 8:15288
99. Rieder CL, Davison EA, Jensen LCW, Cassimeris L, Salmon ED. 1986. Oscillatory movements of monooriented chromosomes and their position relative to the spindle pole result from the ejection properties of the aster and half-spindle. *J. Cell Biol.* 103:581–91
100. Roof DM, Meluh PB, Rose MD. 1992. Kinesin-related proteins required for assembly of the mitotic spindle. *J. Cell Biol.* 118:95–108
101. Sanchez T, Chen DTN, DeCamp SJ, Heymann M, Dogic Z. 2012. Spontaneous motion in hierarchically assembled active matter. *Nature* 491:431–34
102. Sauer G, Körner R, Hanisch A, Ries A, Nigg EA, Silljé HH. 2005. Proteome analysis of the human mitotic spindle. *Mol. Cell. Proteom.* 4:35–43
103. Sawin KE, LeGuellec K, Philippe M, Mitchison TJ. 1992. Mitotic spindle organization by a plus end-directed microtubule motor. *Nature* 359:540–43
104. Sawin KE, Mitchison TJ. 1991. Poleward microtubule flux mitotic spindles assembled in vitro. *J. Cell Biol.* 112:941–54
105. Schermelleh L, Heintzmann R, Leonhardt H. 2010. A guide to super-resolution fluorescence microscopy. *J. Cell Biol.* 190:165–75

106. Sharp DJ, Yu KR, Sisson JC, Sullivan W, Schoely JM. 1999. Antagonistic microtubule-sliding motors position mitotic centrosomes in *Drosophila* early embryos. *Nat. Cell Biol.* 1:51–54
107. Shelley MJ. 2016. The dynamics of microtubule/motor-protein assemblies in biology and physics. *Annu. Rev. Fluid Mech.* 48:487–506
108. Shimamoto Y, Maeda YT, Ishiwata S, Libchaber AJ, Kapoor TM. 2011. Insights into the micromechanical properties of the metaphase spindle. *Cell* 145:1062–74
109. Shinar T, Mana M, Piano F, Shelley MJ. 2011. A model of cytoplasmically driven microtubule-based motion in the single-celled *Caenorhabditis elegans* embryo. *PNAS* 108:10508–13
110. Simha RA, Ramaswamy S. 2002. Hydrodynamic fluctuations and instabilities in ordered suspensions of self-propelled particles. *Phys. Rev. Lett.* 89:058101
111. Skoufias DA, DeBonis S, Saoudi Y, Lebeau L, Crevel I, et al. 2006. S-Trityl-L-cysteine is a reversible, tight binding inhibitor of the human kinesin Eg5 that specifically blocks mitotic progression. *J. Biol. Chem.* 281:17559–69
112. Surrey T, Nédélec F, Leibler S, Karsenti E. 2001. Physical properties determining self-organization of motors and microtubules. *Science* 292:1167–71
113. Szent-Györgyi A. 1943. Observations on actomyosin. *Stud. Inst. Med. Chem. Univ. Szeged* 3:86–92
114. Takagi J, Itabashi T, Suzuki K, Shimamoto Y, Kapoor TM, Ishiwata S. 2014. Micromechanics of the vertebrate meiotic spindle examined by stretching along the pole-to-pole axis. *Biophys. J.* 106:735–40
115. Tanaka F, Edwards SF. 1992. Viscoelastic properties of physically cross-linked networks. 1. Transient network theory. *Macromolecules* 25:1516–23
116. Tirnauer JS, Salmon ED, Mitchison TJ. 2004. Microtubule plus-end dynamics in *Xenopus* egg extract spindles. *Mol. Biol. Cell* 15:1776–84
117. Tólic-Nørrelykke IM. 2008. Push-me-pull-you: how microtubules organize the cell interior. *Eur. Biophys. J.* 37:1271–78
118. Tólic-Nørrelykke IM, Sacconi L, Thon G, Pavone FS. 2004. Positioning and elongation of the fission yeast spindle by microtubule-based pushing. *Curr. Biol.* 14:1181–86
119. Uteng M, Hentrich C, Miura K, Bieling P, Surrey T. 2008. Poleward transport of Eg5 by dynein-dynactin in *Xenopus laevis* egg extract spindles. *J. Cell Biol.* 182:715–26
120. Valentine MT, Fordyce PM, Krzysiak TC, Gilbert SP, Block SM. 2006. Individual dimers of the mitotic kinesin motor Eg5 step processively and support substantial loads in vitro. *Nat. Cell Biol.* 8:470–76
121. Valentine MT, Perlman ZE, Mitchison TJ, Weitz DA. 2005. Mechanical properties of *Xenopus* egg extract cytoplasmic extracts. *Biophys. J.* 88:680–89
122. Verde F, Berrez JM, Antony C, Karsenti E. 1991. Taxol-induced microtubule asters in mitotic extracts of *Xenopus* eggs: requirement for phosphorylated factors and cytoplasmic dynein. *J. Cell Biol.* 112:1177–87
123. Verde F, Dogterom M, Stelzer E, Karsenti E, Leibler S. 1992. Control of microtubule dynamics and length by cyclin A- and cyclin B-dependent kinases in *Xenopus* egg extracts. *J. Cell Biol.* 118:1097–108
124. Walczak CE, Cai S, Khodjakov A. 2010. Mechanisms of chromosome behaviour during mitosis. *Nat. Rev. Mol. Cell Biol.* 11:91–102
125. Waterman-Storer C, Desai A, Salmon ED. 1999. Fluorescent speckle microscopy of spindle microtubule assembly and motility in living cells. *Metb. Cell Biol.* 61:155–73
126. Weisenberg R, Cianci C. 1984. ATP-induced gelation-contraction of microtubules assembled in vitro. *J. Cell Biol.* 99:1527–33
127. Wu HY, Nazockdast E, Shelley MJ, Needleman JD. 2016. Forces positioning the mitotic spindle: theories, and now experiments. *BioEssays* 39:1600212
128. Wühr M, Dumont S, Groen AC, Needleman DJ, Mitchison TJ. 2009. How does a millimeter-sized cell find its center? *Cell Cycle* 8:1115–21
129. Wühr M, Freeman RMJ, Presler M, Horb ME, Peshkin L, et al. 2014. Deep proteomics of the *Xenopus laevis* egg using an mRNA-derived reference database. *Curr. Biol.* 24:1467–75
130. Yu CH, Langowitz N, Wu HY, Farhadifar R, Brugués J, et al. 2014. Measuring microtubule polarity in spindles with second-harmonic generation. *Biophys. J.* 106:1578–87

Contents

Structural Basis for G Protein–Coupled Receptor Signaling <i>Sarah C. Erlandson, Conor McMabon, and Andrew C. Kruse</i>	1
Collapse Transitions of Proteins and the Interplay Among Backbone, Sidechain, and Solvent Interactions <i>Alex S. Holehouse and Robit V. Pappu</i>	19
Measuring Entropy in Molecular Recognition by Proteins <i>A. Joshua Wand and Kim A. Sharp</i>	41
Assembly of COPI and COPII Vesicular Coat Proteins on Membranes <i>Julien Bébune and Felix T. Wieland</i>	63
Imaging mRNA In Vivo, from Birth to Death <i>Evelina Tutucci, Nathan M. Livingston, Robert H. Singer, and Bin Wu</i>	85
Nanodiscs: A Controlled Bilayer Surface for the Study of Membrane Proteins <i>Mark A. McLean, Michael C. Gregory, and Stephen G. Sligar</i>	107
The Jigsaw Puzzle of mRNA Translation Initiation in Eukaryotes: A Decade of Structures Unraveling the Mechanics of the Process <i>Yaser Hashem and Joachim Frank</i>	125
Hemagglutinin-Mediated Membrane Fusion: A Biophysical Perspective <i>Sander Boonstra, Jelle S. Blijleven, Wouter H. Roos, Patrick R. Onck, Erik van der Giessen, and Antoine M. van Oijen</i>	153
Cryo-EM Studies of Pre-mRNA Splicing: From Sample Preparation to Model Visualization <i>Max E. Wilkinson, Pei-Chun Lin, Clemens Plaschka, and Kiyoshi Nagai</i>	175
Structure and Dynamics of Membrane Proteins from Solid-State NMR <i>Venkata S. Mandala, Jonathan K. Williams, and Mei Hong</i>	201
The Molecular Origin of Enthalpy/Entropy Compensation in Biomolecular Recognition <i>Jerome M. Fox, Mengxia Zhao, Michael J. Fink, Kyungtae Kang, and George M. Whitesides</i>	223

Modeling Cell Size Regulation: From Single-Cell-Level Statistics to Molecular Mechanisms and Population-Level Effects <i>Po-Yi Ho, Jie Lin, and Ariel Amir</i>	251
Macroscopic Theory for Evolving Biological Systems Akin to Thermodynamics <i>Kunibiko Kaneko and Chikara Furusawa</i>	273
Photoreceptors Take Charge: Emerging Principles for Light Sensing <i>Tilman Kottke, Aibua Xie, Delmar S. Larsen, and Wouter D. Hoff</i>	291
High-Resolution Hydroxyl Radical Protein Footprinting: Biophysics Tool for Drug Discovery <i>Janna Kiselar and Mark R. Chance</i>	315
Dynamic Neutron Scattering by Biological Systems <i>Jeremy C. Smith, Pan Tan, Loukas Petridis, and Liang Hong</i>	335
Hydrogel-Tissue Chemistry: Principles and Applications <i>Viviana Gradinaru, Jennifer Treweek, Kristin Overton, and Karl Deisseroth</i>	355
Serial Femtosecond Crystallography of G Protein–Coupled Receptors <i>Benjamin Stauch and Vadim Cherezov</i>	377
Understanding Biological Regulation Through Synthetic Biology <i>Caleb J. Bashor and James J. Collins</i>	399
Distinct Mechanisms of Transcription Initiation by RNA Polymerases I and II <i>Christoph Engel, Simon Neyer, and Patrick Cramer</i>	425
Dynamics of Bacterial Gene Regulatory Networks <i>David L. Shis, Matthew R. Bennett, and Oleg A. Igoshin</i>	447
Molecular Mechanisms of Fast Neurotransmitter Release <i>Axel T. Brunger, Ucheor B. Choi, Ying Lai, Jeremy Leitz, and Qiangjun Zhou</i>	469
Structure and Immune Recognition of the HIV Glycan Shield <i>Max Crispin, Andrew B. Ward, and Ian A. Wilson</i>	499
Substrate-Induced Formation of Ribosomal Decoding Center for Accurate and Rapid Genetic Code Translation <i>Michael Y. Pavlov and Måns Ehrenberg</i>	525
The Biophysics of 3D Cell Migration <i>Pei-Hsun Wu, Daniele M. Gilkes, and Denis Wirtz</i>	549
Single-Molecule View of Small RNA–Guided Target Search and Recognition <i>Viktorija Globyte, Sung Hyun Kim, and Chirlmin Joo</i>	569

Behavioral Variability and Phenotypic Diversity in Bacterial Chemotaxis <i>Adam James Waite, Nicholas W. Frankel, and Thierry Emonet</i>	595
Mechanotransduction by the Actin Cytoskeleton: Converting Mechanical Stimuli into Biochemical Signals <i>Andrew R. Harris, Pamela Freij, and Daniel A. Fletcher</i>	617
The Physical Properties of Ceramides in Membranes <i>Alicia Alonso and Félix M. Goñi</i>	633
The Physics of the Metaphase Spindle <i>David Oriola, Daniel J. Needleman, and Jan Brugués</i>	655

Indexes

Cumulative Index of Contributing Authors, Volumes 43–47	675
---	-----

Errata

An online log of corrections to *Annual Review of Biophysics* articles may be found at
<http://www.annualreviews.org/errata/biophys>